JOURNAL OF AEROSPACE COMPUTING, INFORMATION, AND COMMUNICATION
Vol. 1, November 2004

Neural Network Based Algorithms for Comprehensive Collective Axis Limit Avoidance on Rotorcraft

Nilesh A. Sahani* and Joseph F. Horn†
Pennsylvania State University, University Park, Pennsylvania 16802

Military rotorcraft are constrained by a number of operational limits designed to protect the structural integrity and controllability of the aircraft. There is interest in developing advanced control systems that provide Carefree Maneuvering capability on future rotorcraft, so that pilots can fly the entire flight envelope without requiring excessive workload to monitor limits. Recent advances in numerical algorithms and computing technologies such as neural networks are valuable tools in the implementation of such a control system. The present work is focused on developing advanced prediction algorithms for a comprehensive collective axis limit avoidance system for rotorcraft. The system is designed to simultaneously prevent exceedances of the continuous and transient transmission torque limits, transient RPM limit and engine temperature torque limit. The system is also used to assist in One Engine Inoperative (OEI) recovery and autorotation. A dynamic trim estimation algorithm using offline trained neural networks and polynomial curve-fits for torque prediction is used to calculate constraints on the collective stick for continuous torque limits. Different configurations of torque prediction are evaluated for possible implementation in existing and future rotorcraft. A peak response estimation algorithm based on linear model of aircraft dynamics is used for transient limit prediction. The system is tested using a high fidelity, non-linear simulation model of the UH-60A Black Hawk helicopter. Results were generated for a variety of maneuvers in non-real-time simulations using a simple feedback controller to simulate the pilot. A stick limiting method that combines the precision of Automatic Flight Control System (AFCS) limiting with the limit over-ride capability of tactile cueing is proposed.

Nomenclature

A, b, C	=	state space dynamic matrices
e, e_{qs}	=	error signals
E_1, E_2	=	output response parameters
K_{omg}	=	proportional feedback gain, ft-lb-s/rad
P_{amb}, T_{amb}	=	ambient temperature and pressure, psi, Rankine
Q	=	total torque, ft-lb
Q_{actual}	=	measured torque, ft-lb
Q_{pred}, $Q_{predicted}$	=	torque predicted by neural network, ft-lb
$Q_{EngineTemp}$, Q_{OEI}	=	engine temperature and One Engine Inoperative torque limit, ft-lb
$u, v, w, p, q, r, \varphi, \theta, \psi$	=	body velocities, angular rates and Euler angles, ft/s, rad/s, deg
u	=	control input vector (stick displacement)
V_x, V_y, V_z	=	x, y, z components of air velocity at main rotor hub, ft/s
V_{tot}, V_d	=	total and descent velocity, ft/s
x	=	state vector
y	=	output vector

Received 4 November 2003; revision received 29 April 2004; accepted for publication 13 September 2004.

*Graduate Research Assistant, Department of Aerospace Engineering.
†Assistant Professor, Department of Aerospace Engineering.

Δ	=	variation from trim position
Ω	=	rotor rpm, rad/s
ρ	=	air density, lb/ft^3
δ_{col}, δ_{ped}	=	collective and pedal position, in
δ_{col}^{*}	=	critical control position, in
δ_{col}^{eff}	=	stick response to pilot input for stick limiting, in

Subscripts:

0	=	initial condition / normal operating condition
e	=	trim value
lim	=	limiting value
highlim, lowlim	=	upper and lower limit values

I. Introduction

RECENTLY there has been increased interest in achieving carefree handling / maneuvering (CFM) on modern rotorcraft through the use of advanced flight controls and cueing systems. The terms "Carefree Handling" or "Carefree Maneuvering" refer to the capability of a pilot to fly throughout the operational flight envelope without requiring significant workload to monitor and avoid exceeding structural, aerodynamic or control limits.[1] A number of studies have shown that handling qualities are degraded as pilots attempt to perform aggressive maneuvers, and this is largely due to the requirement to monitor and avoid envelope limits associated with the structural, controllability, and engine performance constraints on the aircraft.[1-4] Pilots must typically be conservative when maneuvering near structural limits that are not easily perceived. The operational effectiveness, safety, and reliability of military rotorcraft would be increased if pilots could fly the full envelope without concern for limits.[4] A number of novel systems have been developed that predict the onset of limits and then cue the pilots of approaching limits using tactile feedback.[5-14] Tactile cueing allows the pilot to maneuver to the edge of the envelope while keeping their eyes and concentration focused on performing the desired task. In addition to cueing, there is also the potential of addressing envelope limits in the AFCS or through a combination of cueing and AFCS limiting.[3]

Limit prediction algorithms often play a critical role in carefree maneuvering (CFM) systems. The algorithms are used to predict the onset of limits and to calculate the allowable control motion in order to avoid the limit. Recent advances in numerical algorithms and computing technologies such as neural networks are valuable tools in designing the prediction algorithms needed for CFM control systems. The present work presents a number of advances and improvements on prediction algorithms previously developed in Refs. 6-12. The algorithms are used for a comprehensive collective axis limit avoidance system on a military helicopter. A subset of the systems presented here was used in a tactile cueing system tested in piloted simulation.[13] In the present study, the system is used for providing envelope limiting through the Automatic Flight Control System (AFCS) by constraining the collective input. The system is tested in non-realtime simulation using a high fidelity non-linear simulation model of the UH-60A helicopter.

II. Collective Axis Limit Avoidance System

The two most critical parameters associated with the collective axis are torque and rotor speed. The torque response to the collective control consists of both a transient oscillation and a steady-state response. The transient torque should not exceed the absolute torque limit of the transmission. The steady-state torque limit should not exceed the continuous torque limit of transmission for a significant amount of time. Exceeding the transient limit for any period of time, or exceeding the continuous torque limit for an extended period of time can result in damage to the gearbox. This will reduce the life of the gearbox and can potentially result in a failure. In certain situations, the engine torque limit might be more critical than the transmission limit. The engine torque limit is associated with the maximum allowable temperature in the turbine, and is a function of ambient conditions. The engine fuel controller is designed to prevent the engines from exceeding the turbine temperature limit by limiting the fuel flow to the engine. Therefore, if the pilot applies a collective input that causes the engine torque limit to be exceeded, the engine cannot supply the torque required by the rotor to rotate at the given RPM. This results in a droop in the rotor RPM. The engine torque limit becomes important in One Engine Inoperative (OEI) condition, i.e. when one engine fails to operate, or when operating in high altitude/hot day condition. Also, collective stick inputs cause fluctuations in RPM

due to changing torque levels. Large fluctuations in RPM can create rotor stability and controllability problem in rotorcraft.

A schematic of the collective axis carefree maneuvering system is shown in Fig. 1. Transmission torque limit and engine temperature limit are steady-state torque limits. A neural network based dynamic trim prediction algorithm[6] is used for predicting the steady-state limits. A peak response estimation algorithm[7] using a linear model of aircraft dynamics is used for predicting the transient limits associated with transient torque and transient RPM. These prediction algorithms generate the upper and lower limits on the collective stick. These limits can be used to generate tactile cues or can be used by the AFCS to ensure limits are not exceeded.

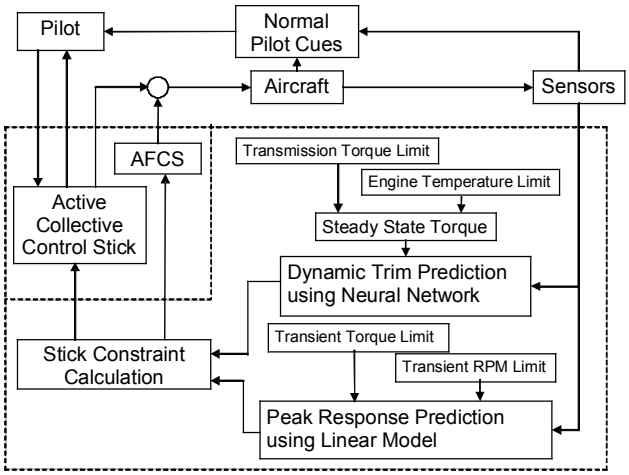

Fig. 1 Schematic of collective stick limit avoidance system.

III. Continuous Torque Limit

A. System Implementation

A schematic implementation of the continuous torque limit avoidance system is shown in Fig. 2. A dynamic trim prediction algorithm detailed in Ref. 6 is used for predicting the continuous torque limit. The algorithm requires a functional representation of quasi-steady torque in trim flight condition. Analytical equations for calculating the torque are relatively complex, computationally intensive and are not suitable for implementing in realtime. Conventional methods like table lookup are not feasible for representing nonlinear functions with large number of variables over a wide range of operating condition. Neural Networks offer the best alternative solution because of their computational efficiency and their ability to map complex non-linear functions with required accuracy. The data required for training the neural network can be generated using a simulation model or flight test data. There are concerns that neural network adds complexity to the control system, and makes software validation difficult. For this purpose, a simple polynomial curve fit can be used for function approximation instead of a neural network. For the present study, both neural networks and polynomial curve fits are investigated. However, an analytical model or table look-up could also be used.

The quasi-steady torque is a function of aircraft states and control inputs:

$$Q_{pred} = f(\mathbf{x},\mathbf{u}) \tag{1}$$

It can be assumed that the torque coefficient remains constant with altitude. Thus, it suffices to generate the training data at a constant altitude. The torque predicted by the neural network can then be scaled by the density ratio to adjust the difference between the actual altitude and the prediction altitude. It is also scaled by the rotor speed to adjust changes in rotor speed:

$$Q_{predicted} = Q_{pred}\,\frac{\rho}{\rho_0}\left(\frac{\Omega}{\Omega_0}\right)^2 \tag{2}$$

The predicted torque of the neural net will not always be accurate due to modeling errors, variation in weight and mass properties, and the variation in the performance of different aircraft and rotor systems. The adaptive scheme developed by Bateman et al.[14] is used for correcting the predicted torque. The adaptation algorithm accounts for low-frequency errors in actual quasi-steady torque and the torque predicted by the neural net. The corrected torque is compared with the limiting torque (Q_{lim}). The limiting torque is the most restrictive of all the quasi-steady torque limits. For normal operating condition, it is the minimum of the gearbox transmission limit and the engine temperature torque limit. Computing the torque limit under the special operating conditions of One Engine Inoperative (OEI) recovery and autorotation will be explained in the following sections.

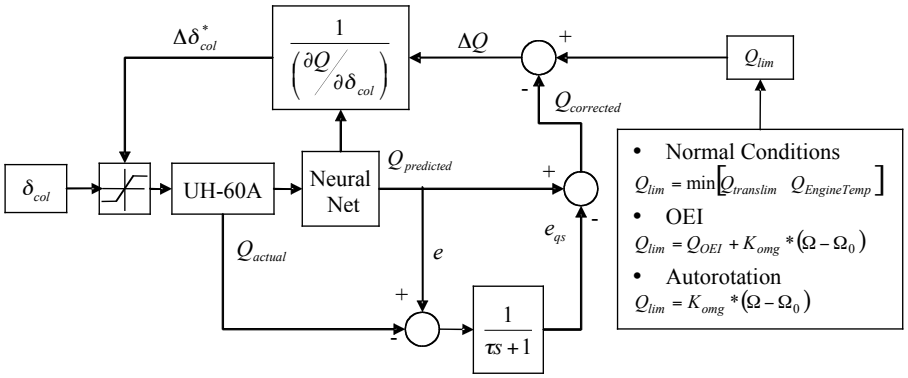

Fig. 2 Schematic representation of continuous torque limit avoidance algorithm.

To determine the critical control margin vector, the function *f* in Eq. (1) is linearized at the operating point using the Taylor series expansion.

$$y(\mathbf{x}, \mathbf{u} + \Delta\mathbf{u}) = f(\mathbf{x}, \mathbf{u}) + \frac{\partial f}{\partial \mathbf{u}} \Delta\mathbf{u} + \text{H.O.T.} \tag{3}$$

The proximity of the limit boundary is approximated from the linearized equations as the sensitivity of function *f* to the controls. Since we are only interested in the collective stick margin, the previous sensitivity function is evaluated only for the collective stick position. It is evaluated numerically from the neural net as a first order central difference:

$$\frac{\partial f}{\partial \delta_{col}} = \lim_{\Delta\delta_{col} \to 0} \frac{f(\mathbf{x}, \delta_{ped}, \delta_{col} + \Delta\delta_{col}) - f(\mathbf{x}, \delta_{ped}, \delta_{col} - \Delta\delta_{col})}{2\Delta\delta_{col}} \tag{4}$$

Dividing the torque difference by the collective stick sensitivity gives the collective stick control margin:

$$\Delta\delta^*_{col} = \frac{\Delta Q}{\partial f / \partial \delta_{col}} \tag{5}$$

The sum of the control margin and the current stick position gives the limiting stick position:

$$\delta^*_{col} = \delta_{col} + \Delta\delta^*_{col} \tag{6}$$

B. Neural Network Training and Implementation

The data required for training the neural network can be obtained using flight tests or a simulation model. For the present work, a simulation model of the UH-60A Black Hawk (GENHEL)[15] is used. The data is generated for various trim conditions. The objective is to include all the flight conditions that might be encountered in a dynamic trim flight. For the given weight and velocity, the vertical flight path angle is varied through 180 deg to cover descent and climb conditions and horizontal flight path angle is varied through 360 deg to cover the forward flight,

side-slip and backward flight. These angles are varied independent of others to cover the velocity vector in all the three dimensions. The velocity is varied from zero to 140 knots and weight is varied from 11000 lb to 20000 lb. The velocity and weight are varied independently and for each case the flight path angles are varied to cover all the data points. This data covers the trim points for straight-line flight. To cover the trim data for turning flight, the same procedure is repeated with various turning rates. The turning rates of up to ±30 degree/sec are considered. With this procedure, around 43000 data points are generated. The number of data points reduces with increasing velocity as the aircraft looses the capability to trim at these extreme flight conditions.

MATLAB® is used to train a 3-layer feed forward neural net. A hyperbolic tangent basis function is used in first two layers with 8 neurons in the first layer and 5 neurons in the second layer. A linear basis function with one neuron is used for the third layer. The neural network inputs are normalized with respect to their minimum and maximum values to generate the data range between -1 and 1. A Levenberg-Marquardt back-propagation algorithm is used for training of the network.

Using a large number of variables as inputs to the neural net increases their accuracy, but reduces the computational efficiency. Since this algorithm needs to be implemented in real time, the computational efficiency plays an important role in determining the number of input variables. Furthermore, sensors required to measure these input variables put constraints on the selection of variables. In this study, four different methods of torque prediction have been evaluated. The data generation and training procedure is the same for all the neural networks.

C. Methods of Torque Prediction

Four different methods of torque prediction have been considered in the present work. Methods 1, 2 and 3 use neural networks, while Method 4 uses polynomial curve fit for function approximation. Regression plots for each method are shown in Figs. 3-6. A prediction error comparison of the methods is shown in Fig. 7. The figure compares percentage error and Root Mean Squared (RMS) Error in the torque prediction.

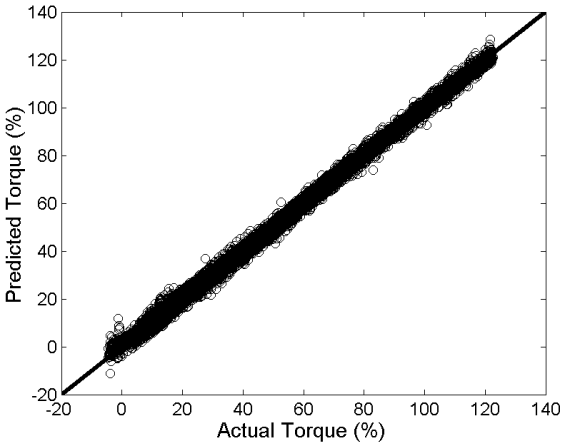

Fig. 3 Regression plot using Method 1.

Method 1: Air Velocities at Hub and Control Inputs

The torque prediction function in Eq. (1) can be represented using three components of air velocity at main rotor hub and collective and pedal position:

$$Q_{pred} = f\left(V_x, V_y, V_z, \delta_{col}, \delta_{ped}\right) \tag{7}$$

where V_x, V_y, V_z are the local velocities at the main rotor hub and, δ_{col} and δ_{ped} are collective and pedal positions respectively. Figure 3 shows the regression plot for the trained neural net. It shows the comparison between the predicted values of the neural net and the actual training data used for training the neural net. As shown in Fig. 7, the error in torque prediction is less than 3.8% for 99% of the data. The Root Mean Squared (RMS) Error for the entire dataset is 1% for this method.

This neural net represents a fairly accurate model for torque prediction. The collective and pedal stick positions can be easily measured, but measuring air velocities at the hub is a difficult task. It requires a low airspeed

measurement system in the hub which is rotating at very high speed. Even though this neural net provides good results with the simulation model, the required sensor upgrading makes it very expensive for practical implementation. Such a system might be available on future aircraft, but we should consider other models which are easier to implement on existing aircraft without sacrificing much accuracy of prediction.

Method 2: Total Velocity, Yaw Rate, Descent Velocity and Control Input

This model uses total velocity, V_{tot}, descent velocity, V_d, yaw rate, $\dot{\psi}$, collective position, δ_{col}, and pedal position, δ_{ped}, as input variables:

$$Q_{pred} = f\left(V_{tot}, V_d, \dot{\psi}, \delta_{col}, \delta_{ped}\right) \tag{8}$$

The total velocity can be measured using a pitot tube. The descent velocity can be measured using a vertical speed measurement system, which measures the rate of change of barometric altitude. Yaw rate can be measured using a rate gyro. The collective stick and pedal positions can also be easily measured. All of the required variables can be measured using sensors that are typically installed on an aircraft. Hence, this model is suitable for practical implementation on existing aircraft. The regression plot for this Neural Net is shown in Fig. 4. The error is less than 6.1% for 99% of the data, and the RMS error for the entire dataset is 1.5%.

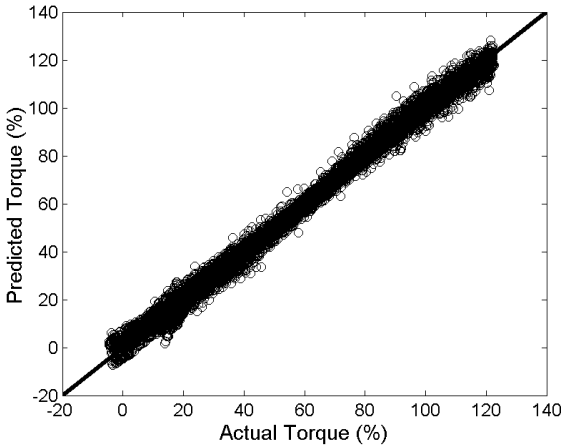

Fig. 4 Regression plot using Method 2.

Method 3: Low Velocity Correction Model

The neural net discussed previously provides a good solution for practical implementation of the torque limiting algorithm. The total velocity can be measured using a pitot tube. However, for rotorcraft operating in hover and low speed flight, the pitot tube measurement can be contaminated by rotor downwash effects. Also, pitot tubes are not very accurate at measuring low airspeeds. Hence, accurate measure of velocity may not be available for these flying conditions. Typically, no airspeed measurement is possible below a certain threshold. In this case, we assume the airspeed measurement shows 30 knots for all flights below 30 knots speed. Above 30 knots, the pitot tube is out of the rotor downwash and velocity indicator shows the actual velocity.

Since, only velocities above 30 knots are available for measurement, a correction is needed for training the neural network. All velocities below 30 knots are treated as 30 knots while training the network.

$$\begin{aligned} 0 < V_{tot}\big|_{measured} < 30kts &\Rightarrow V_{tot} = 30kts \\ 30kts < V_{tot}\big|_{measured} &\Rightarrow V_{tot} = V_{tot}\big|_{measured} \end{aligned} \tag{9}$$

The regression plot for this correction model is shown in Fig. 5. The error is less than 5.7% for 99% of the data, and the RMS error for the entire dataset is 1.5%. The error is actually slightly better than that of Method 2 despite the fact that the network has no specific airspeed information below 30 knots. In this evaluation, about 50% of the data points were below 30 knots. The RMS error for the data point below 30 knots was 1%, compared to 0.63% for

Method 2. It should be noted that the torque prediction is a function of five variables, including collective input and rate of descent, which have a much larger effect on torque than the airspeed in the low speed flight regime. A number of random factors such as the total number training cycles and the initial guess of the network weights can have small effects on the final error results. One can assume that the low velocity correction has essentially no effect on the accuracy of the torque prediction. The method is more practical for implementation on existing aircraft where low airspeed data is not available.

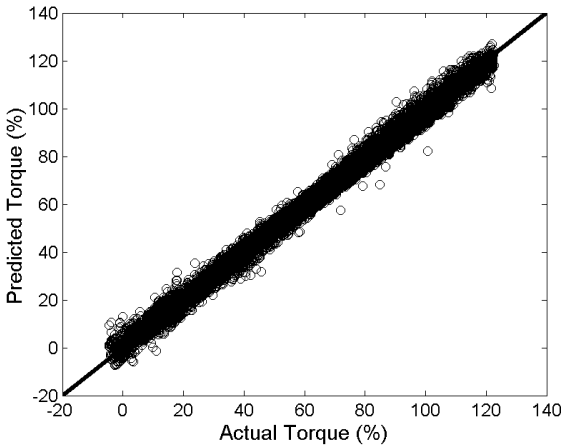

Fig. 5 Regression plot using Method 3.

Method 4: Second Order Curve Fit

The neural network offers a novel way to represent complex non-linear functions. However, there are concerns that neural networks add complexity to the control system, and may make software validation more difficult. A simple second order polynomial curve-fit may be a viable alternative to the neural network. It uses the same input variables as defined in Eq. (8). The equation representing this second order curve fit is:

$$x = [V_{tot}, V_d, \dot{\psi}, \delta_{col}, \delta_{ped}]^T$$

$$Q_{pred} = x^T Ax + Bx + C$$

where

$$A = \begin{bmatrix} -0.51 & -17.3 & -0.26 & -1.75 & -0.35 \\ 0 & -1233.8 & -16.3 & -13.46 & 123.9 \\ 0 & 0 & -0.24 & 3.02 & -0.12 \\ 0 & 0 & 0 & 7.98 & -1.18 \\ 0 & 0 & 0 & 0 & 0.92 \end{bmatrix}$$

$$B = \begin{bmatrix} 138.31 & -6454.6 & -168.49 & 123.31 & -90.96 \end{bmatrix} \quad (10)$$

$$C = 9461.5$$

The total velocity is measured in knots, descent velocity is measured in ft/sec, yaw rate is measured in rad/sec and collective and pedal positions are measured in percentage position. The regression plot for this curve-fit is shown in Fig. 6. The RMS error for this curve fit is 3.3%. The error is less than 12.7% for 99% of the data and within 7% for 95% of the data. This implies that this curve fit provides sufficient accuracy over most of the dataset. There is a noticeable scatter of prediction error at lower torque values. These data points are associated with small descent angles in high speed forward flight. Inaccuracies at these flight conditions might not be critical since the torque values are relatively low and the aircraft would not be flying near a limit.

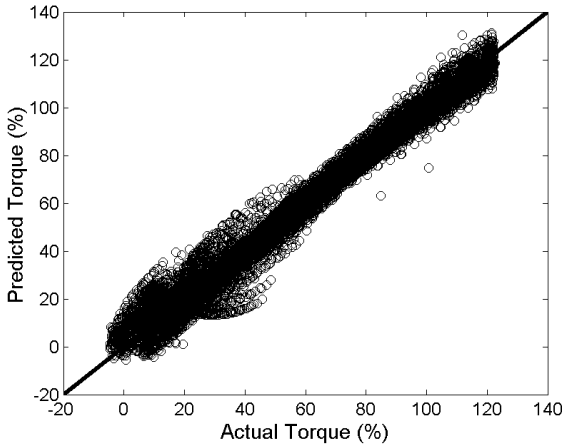

Fig. 6 Regression plot using Method 4.

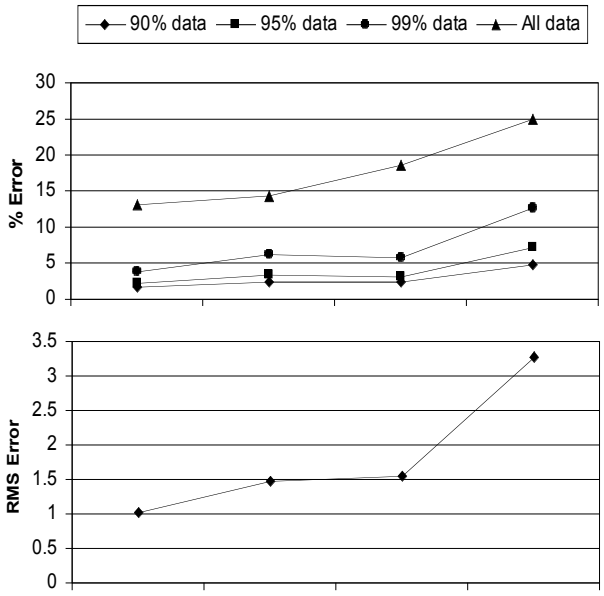

Fig. 7 Prediction error comparison.

IV. Engine Temperature Limit

In normal operating conditions the transmission torque limit is critical. But, when operating in a high altitude / hot day condition, the engine temperature limit is important. The engine torque is limited by the maximum allowable temperature in turbine. The turbine temperature depends on the ambient temperature and pressure as well as the torque output of the engine. This limit is most critical when operating at high altitudes on a hot day.

In normal operating condition, the engine fuel controller works as an RPM governor. It adjusts the fuel flow rate to keep the rotor RPM constant. But, when the turbine temperature approaches its critical value, the fuel controller adjusts the fuel flow rate to keep the turbine temperature below the critical temperature limit. In this condition, if the pilot performs a maneuver that requires more torque than the engine can provide, the rotor RPM droops. The droop in rotor RPM can cause a significant controllability problem. Hence, it is necessary to predict the maximum engine torque available corresponding to the critical temperature limit at the given operating conditions.

The maximum available engine torque is modeled as a function of ambient temperature and pressure:

$$Q_{EngineTemp} = g(P_{amb}, T_{amb}) \tag{11}$$

For the present study, the turbine temperature limit is set to 2004°R. A set of engine torque and turbine temperature data points were generated for various inlet temperatures and pressures. A second order polynomial is used to correlate the engine torque limit as a function of ambient temperature and pressure:

$$Q_{EngineTemp} = 17378P_{amb} + 526.43T_{amb} - 0.89844P_{amb}^{2} - 23.615P_{amb}T_{amb} - 0.47399T_{amb}^{2} - 146{,}110 \tag{12}$$

where, pressure is in psi, temperature is in degree Rankine and torque is in ft-lb.

V. One Engine Inoperative Limit

The One Engine Inoperative (OEI) limit corresponds to the maximum available torque when one engine fails to operate. In this operating condition, the objective is to recover quickly from the OEI without significant loss of altitude. If the aircraft is climbing at low speed (for example during a takeoff) one engine will not provide sufficient power to continue climbing. To recover from OEI, the pilot needs to trade the potential energy for the kinetic energy by descending. After reaching the power bucket, the pilot can start climbing again. Throughout the maneuver, the operational engine is operating at its highest capacity and the engine temperature limit is important. During the recovery from OEI emergencies, the strategy is often to hold the rotor RPM at some optimal value for recovery. The pilot should use maximum available power from one engine, which usually corresponds to the rotor RPM drooped to some fixed percentage of the normal operating RPM (for example 95%).

The maximum torque available by both engines for the given ambient temperature and pressure is known from engine temperature limit given in Eq. (12). When one engine fails, only half of this torque is available. Hence the engine temperature torque limit is divided by two to generate the torque limit for OEI recovery:

$$Q_{OEI} = \frac{Q_{EngineTemp}}{2} \tag{13}$$

This torque limit is usually lower than the transmission limit and acts as a critical torque limit for OEI recovery. In any case, the transmission limit can be ignored in this emergency flight condition.

The optimal rotor RPM for recovery through OEI is different from the normal operating RPM. For the present work, 95% of the normal operating RPM is assumed to be the optimal RPM for recovery.[13] A simple proportional controller is applied to the continuous torque limit to adjust the desired RPM:

$$Q_{lim} = Q_{OEI} + K_{omg} * (\Omega - \Omega_0) \tag{14}$$

As discussed previously, when the torque required exceeds the maximum torque available from the engine, the fuel controller stops operating as a RPM governor and switches to a turbine temperature regulator mode, and the RPM is allowed to droop. The amount of RPM droop is directly related to how much the torque required exceeds the engine torque limit. Thus, if the aircraft is operating at the prescribed torque limit, Q_{lim}, then the amount of RPM droop can be regulated by adjusting the torque limit. The simple proportional control law in Eq. (14) achieves this objective. If the RPM is lower than the optimal RPM, the torque limit is lowered, which alleviate the torque load and allows the rotor to speed up. On the other hand, if the rotor is over-speeding, then the torque limit is increased, which slows down the rotor to bring the RPM to the optimal value. For the present work, the gain K_{omg} is selected as 5000ft-lb·s/rad and the optimal RPM for OEI recovery, Ω_0, is 25.65 rad/sec (95%).

VI. Autorotation Limit

In autorotation the descending velocity turns the rotor, so the engines do not need to generate any torque. However, the rotor still generates lift so that the aircraft descends at a constant speed. When both engines in the helicopter fail to operate, the pilot needs to quickly lower the collective in order to keep the rotor RPM constant. The collective axis cueing system will cue the pilot for optimal collective position to reach the autorotation and to maintain a constant RPM in autorotation. Since there is no torque available from engines, the autorotation torque

limit corresponds to the zero torque value. The fluctuations in the RPM are adjusted using the same proportional controller as discussed for the OEI limit. Thus, the autorotation torque limit becomes:

$$Q_{lim} = K_{omg} * (\Omega - \Omega_0) \tag{15}$$

VII. Transient Torque and Transient RPM Limit

The transient torque and transient RPM are peak response critical limits.[7] The peak response critical limits require limiting the transient peak of the response. The algorithm is designed to estimate the transient peak of the limited parameter that occurs immediately after the control input. The algorithm needs only to predict a very near term response of the limited parameter, typically less than two seconds. Hence, the linear model of fast dynamics of the rotorcraft provides sufficient model for the prediction.

The dynamics of the limited parameter can be described as a linear single input single output state variable model:

$$\begin{aligned} \Delta\dot{\mathbf{x}} &= \mathbf{A}\Delta\mathbf{x} + \mathbf{b}\Delta u \\ \Delta y &= \mathbf{C}\Delta\mathbf{x} \end{aligned} \tag{16}$$

where Δy, Δx, and Δu are the perturbation of the limited parameter, the state vector, and the control input from equilibrium:

$$\Delta\mathbf{x} = \mathbf{x} - \mathbf{x}_e; \qquad \Delta u = u - u_e; \qquad \Delta y = y - y_e \tag{17}$$

The response of the previous system to the step input from non-zero initial condition can be written as:

$$\begin{aligned} y(t) &= \Delta y(t) + y_e \\ &= y_e + \mathbf{C}e^{\mathbf{A}t}\Delta\mathbf{x_0} + \mathbf{C}\mathbf{A}^{-1}\left(e^{\mathbf{A}t} - \mathbf{I}\right)\mathbf{b}\Delta u \end{aligned} \tag{18}$$

The initial condition for the output vector can be used in place of the equilibrium value of the output:

$$\begin{aligned} &y_0 \equiv y(0) = y_e + \mathbf{C}\Delta\mathbf{x_0} \\ &y(t) = y_0 + \mathbf{E_1}(t)\Delta\mathbf{x_0} + \mathbf{E}_2(t)\Delta u \\ &\text{where } \mathbf{E_1}(t) = \mathbf{C}\left(e^{\mathbf{A}t} - \mathbf{I}\right) \\ &\text{and } \mathbf{E}_2(t) = \mathbf{C}A^{-1}\left(e^{\mathbf{A}t} - \mathbf{I}\right)\mathbf{b} \end{aligned} \tag{19}$$

The Δu term is the magnitude of a step control input. In the real-time algorithm, at each frame of execution, the current measured (or estimated) value of the state vector and the limited parameter are used as the initial condition. The peak responses can then be expressed as the maximum and/or minimum value of $y(t)$ over some time interval. A constraint on the control (a softstop location) can then be calculated by solving for the magnitude of a control step input that causes the peak response to just reach a limit.

Solve for Δu such that

$$\begin{aligned} &\max_t \left[y_0 + \mathbf{E_1}(t)\Delta\mathbf{x_0} + \mathbf{E}_2(t)\Delta u \right] = y_{highlim} \\ &\text{and} \\ &\min_t \left[y_0 + \mathbf{E_1}(t)\Delta\mathbf{x_0} + \mathbf{E}_2(t)\Delta u \right] = y_{lowlim} \end{aligned} \tag{20}$$

The solution can be achieved using an iterative search algorithm. The solution can be done in a computationally efficient manner by: 1) Calculating offline and storing the values of the E1 and E2 matrices for some time range (for

some set of fixed time intervals), 2) Constraining the search to the maximum control range and using a bisection algorithm with guaranteed convergence. Thus, based on the current value of the limited parameter and state vector (y_0 and $\mathbf{x_0}$), the algorithm finds the control input that causes the limit to be reached in the peak response.

For the present work, a linear model at hover position of the coupled yaw/heave/rotor speed dynamics of the UH-60A presented in Ref. 16 was used. It is a seventh order model that includes the following states: rotor speed, yaw rate, vertical speed, inflow velocity, engine torque, fuel flow, and integrated rotor speed. The control input is the collective stick input. The model structure is shown next in Eq. (21),

$$\begin{bmatrix} 1 & -1 & & & & & \\ & 1 & & & & & \\ & & 1 & & & & \\ -\frac{v_0}{\Omega_0} & & & 1 & & & \\ & & & & 1 & & \\ & & & & & \tau_{w_f} & \\ & & & & & & 1 \end{bmatrix} \begin{bmatrix} \Delta\dot{\Omega} \\ \Delta\dot{r} \\ \Delta\dot{w} \\ \Delta\dot{v} \\ \Delta\dot{Q} \\ \Delta\dot{w}_f \\ \Delta\dot{\Psi} \end{bmatrix} = \begin{bmatrix} R_\Omega & & R_w & -R_w & R_Q & & \\ & N_r & N_w & & N_Q & & \\ Z_\Omega & Z_r & Z_w & -Z_w & & & \\ & & I_w & I_v & & & \\ & & & & T_Q & T_{w_f} & \\ K_P & & & & & -1 & K_I \\ 1 & & & & & & \end{bmatrix} \begin{bmatrix} \Delta\Omega \\ \Delta r \\ \Delta w \\ \Delta v \\ \Delta Q \\ \Delta w_f \\ \Delta\Psi \end{bmatrix} + \begin{bmatrix} R_{col} \\ N_{col} \\ Z_{col} \\ I_{col} \\ T_{col} \\ \\ \end{bmatrix} \Delta\delta_{col} \tag{21}$$

The model structure is well suited for modeling both the transient rotor RPM dynamics and transient torque dynamics. Thus, this same model can be used to implement a peak response estimation algorithm for both the rotor RPM limit and the transient torque limit. It was found that the linear model at hover position also works well at low speeds. Linear models can be scheduled with velocity to improve the accuracy of prediction at higher speeds. It is also possible to replace the E1 and E2 matrices in Eq. (20) by neural networks as a function of flight conditions.

The linear model was extracted from the non-linear simulation response data using frequency domain identification methods. A varying frequency sinusoidal input (a "chirp" input) to the collective stick was simulated, and the frequency response of the torque and rotor speed responses were identified. The parameters in the state-space model shown in Eq. (21) were then derived to fit the linear model frequency response to that of the non-linear simulation model. The Comprehensive Identification from Frequency Responses (CIFER®) software was used for this purpose.[17] CIFER® has proven to be a powerful tool in the aerospace industry (particular in the rotorcraft sector) for deriving accurate linear models for use in flight control design, and it was found that this tool was also well suited for extracting a linear model for the peak response estimation algorithm. Figures 8 and 9 show the frequency response identified from the non-linear model compared to that of the linear model used in the algorithm as calculated by CIFER®. There is reasonable correlation in the frequency responses.

VIII. Limit Avoidance

The constraints on the collective stick for quasi-steady limits are calculated using Eq. (6) and for transient limits using Eq. (20). The limit avoidance system must prioritize the various constraints and either cue the pilot appropriately or constrain the pilot control input through the AFCS. The algorithms presented previously are independent of the method used for limit avoidance. The actual implementation of a cueing system depends on the pilot preferences and must be designed based on piloted simulation. This is beyond the scope of present work. For the present study, the stick motion is constrained through the AFCS. In this type of approach, the sensitivity of collective stick to control input is altered. For example, if the pilot is operating near the limit, then the efficiency of collective stick is decreased. This means that pilot needs to put larger stick input to get the desired response. If the pilot control input is δ_{col} then the effective control input observed by the aircraft is δ_{col}^{eff}.

One such stick limiting function, hereafter referred as "Limit Over-ride Approach," is shown in Fig. 10. In this approach, the stick response is divided into three regions: Limiting region, Dead-band region and Recovery region. In the Limiting region the stick sensitivity to the pilot input slowly decreases till it reaches zero at the end of the Limiting region. It is followed by the Dead-band region with zero stick sensitivity. Pilot input in this region does not affect the aircraft response. This region is followed by the Recovery region with increased sensitivity to the collective stick. This region allows the pilot to over-ride the limit in emergency situation. It also recovers the "lost" stick input in Limiting and Dead-band region by allowing higher stick sensitivity. A polynomial function is mapped to represent each region.

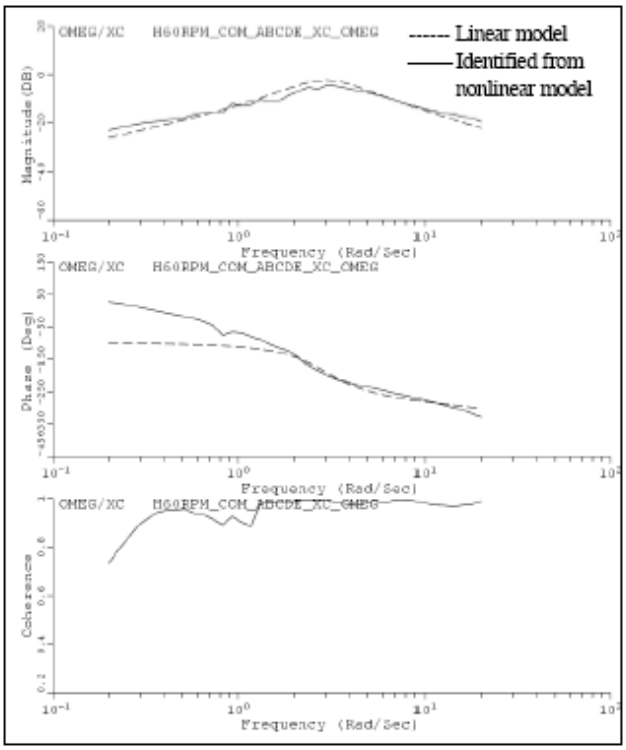

Fig. 8 Linear model of rotor speed response extracted using CIFER®.

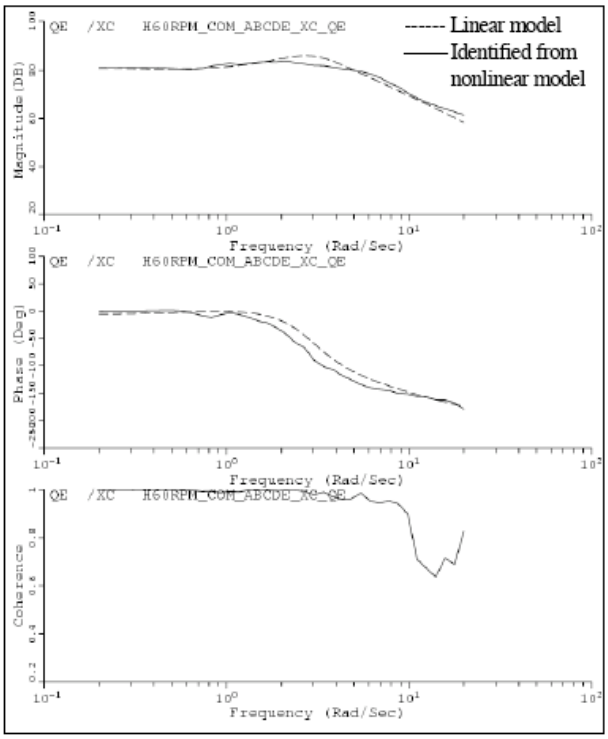

Fig. 9 Linear model of torque response extracted using CIFER®.

In Fig. 10, the points A, B, C and D represent the boundary points for each region. The point L represents the stick limit. The distance x is measured from the limit. This function implemented for the present study has 0.8 inches wide limiting region, 0.4 inches wide dead-band region and 1.5 inches wide recovery region for 10 inches of maximum stick travel. Two boundary conditions are forced at each point:

$$\begin{aligned}
&\text{A}: \quad x = -0.4, y = -0.4 \quad ; \quad \left.\frac{dy}{dx}\right|_A = 1 \\
&\text{B}: \quad x = 0.4, y = 0 \quad ; \quad \left.\frac{dy}{dx}\right|_B = 0 \\
&\text{C}: \quad x = 0.8, y = 0 \quad ; \quad \left.\frac{dy}{dx}\right|_C = 0 \\
&\text{D}: \quad x = 2.3, y = 2.3 \quad ; \quad \left.\frac{dy}{dx}\right|_D = 1
\end{aligned}$$

where

$$\begin{aligned}
x &= \delta_{col} - \delta^*_{col} \\
y &= \delta^{eff}_{col} - \delta^*_{col}
\end{aligned}$$

(22)

The polynomial equation obtained using the previous boundary conditions is represented next:

$$\delta^{eff}_{col} = \begin{cases}
\delta_{col} & \forall \quad x < -0.4 \\
\delta^*_{col} - 0.1 + 0.5x - 0.625x^2 & \forall \quad -0.4 \le x < 0.4 \\
\delta^*_{col} & \forall \quad 0.4 \le x < 0.8 \\
\left\{ \begin{matrix} \delta^*_{col} + 2.006 - 5.6035x \\ +4.604x^2 - 0.9185x^3 \end{matrix} \right\} & \forall \quad 0.8 \le x < 2.3 \\
\delta_{col} & \forall \quad 2.3 \le x
\end{cases}$$

(23)

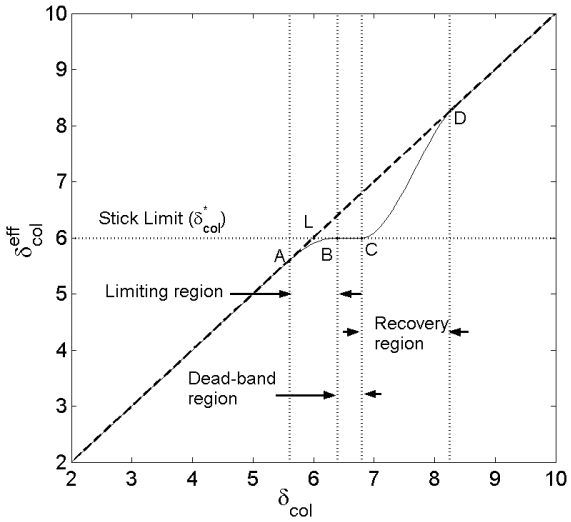

Fig. 10 Limit over-ride approach for constrained stick motion.

This stick function can be implemented using a combination of AFCS limiting and tactile cueing on the stick. The limiting function can be incorporated in the AFCS which modifies the pilot control input. At the same time,

tactile cueing is applied which allows the pilot to discriminate each region. This can be achieved by applying stick shaker cues with distinct frequency for each region. This method for stick limiting combines the precision of AFCS limiting with the limit over-ride capability of stick cueing. Stick shakers are relatively easy to implement and are routinely used on commercial aircrafts for stall warning.

A special case of this limit over-ride approach is a "Dead-band Approach" where the dead band region extends till the end of stick travel without any recovery region. This approach does not allow the pilot to over-ride the limit. Though it is not suitable for implementation in flight, it is most useful for validation and testing of limiting algorithms. This approach has been used in the present work for non-real-time simulations using GENHEL as discussed in the flowing section.

IX. Results

The algorithms discussed in the preceding sections have been tested using the GENHEL[15] simulation of the UH-60A helicopter. All results were performed in non-real-time simulation without a human pilot. Instead, maneuvers are performed using either prescribed control inputs or using a simple pilot model.[12] The pilot model is a feedback controller which uses proportional plus integral compensation to perform a maneuver given lateral, longitudinal and descent velocities. The pilot model effectively calculates the controls required to perform the specified maneuver. In order to test the limiting algorithms, the control inputs are then filtered through the stick limiting functions as discussed in the previous section. In the following discussion, "the pilot" refers to the pilot model and not an actual human pilot.

Figure 11 demonstrates the effectiveness of the algorithms for a simple step input. Here, a simple maneuver is simulated where the pilot starts from hover and gives 3 inches of collective stick spanned over 2 seconds. If no collective stick limiting is applied, torque exceeds the transmission torque limit. Using the dead-band limiting approach, the stick motion follows the collective stick limit boundary. This results in the steady-state torque not exceeding the torque limit. Thus, the pilot can avoid the torque limit by staying within the dead-band region. But, in emergency conditions the pilot can move the stick in the recovery region and can attain almost the same altitude and rate of climb as if there is no stick limiting applied.

Figure 12 shows the comparison of different methods of torque prediction. As discussed before, Method 1 uses air velocities at hub and control inputs while Methods 2, 3, and 4 use total velocity, yaw rate, descent velocity and control inputs as input variables. Methods 1, 2, and 3 use neural net prediction while Method 4 uses a second order curve fit. The figure shows that there is little difference between predictions of each method. This result confirms the fact that approximations made for each method are feasible and have little effect on the torque prediction. Thus, any method can be used for torque prediction depending upon the requirements.

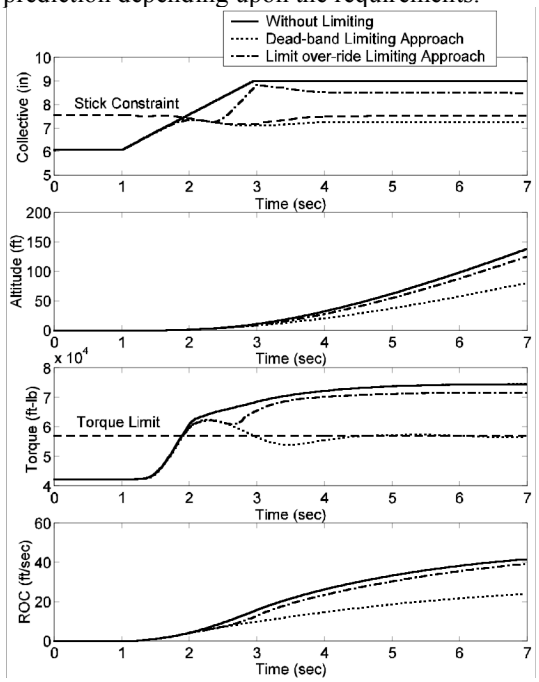

Fig. 11 Comparison of dead-band and limit over-ride stick limiting approaches with no limiting.

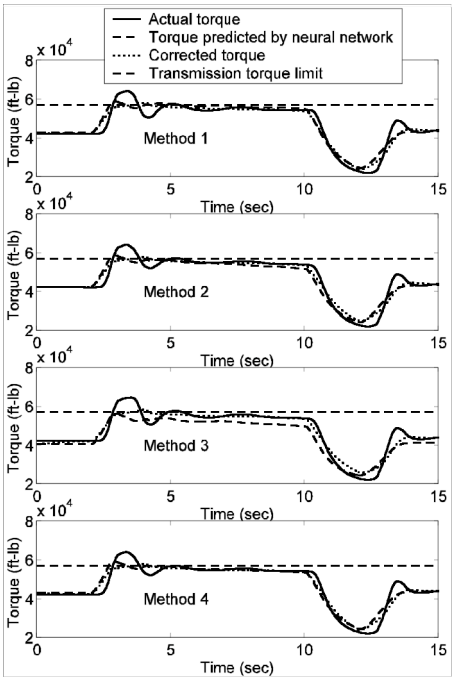

Fig. 12 Comparison of torque prediction methods.

On the UH-60A, the transmission torque limit is critical for most of the operating conditions. But, when operating at high altitude, the engine torque limit is more important. Figure 13 shows the results obtained for simulation of a simple acceleration maneuver. The helicopter starts from hover at 6000ft with the ambient temperature of 113°F and pressure of 13.6psi. At this operating condition, the engine temperature limit is lower than the transmission torque limit. From the hover position, the pilot commands two inches of collective stick input spanned over two seconds. Then the pilot holds the stick at that position for two seconds and then returns it to its hover position in next two seconds. If no stick limiting is applied, torque exceeds the engine temperature limit and even the transmission torque limit. But, if the collective stick follows the limit boundary, torque does not exceed the engine temperature limit.

Figure 14 shows the switching of the continuous torque limit from the transmission torque limit to the engine temperature torque limit as altitude increases. The pilot starts climbing from 5200ft with the ambient temperature of 100°F and pressure of 13.5psi. The pilot commands the climbing rate of 20ft/sec. At this altitude, the pilot hits the transmission torque limit. But, as the aircraft starts gaining the altitude, the engine temperature limit becomes critical. Without the limiting, pilot overlooks the limits which results in large fluctuations in rotor RPM. But, with the limiting the pilot can avoid the large RPM droop.

The OEI limit is tested for Category A takeoff maneuver. The Category A takeoff maneuver starts with the helicopter in hover over the rooftop of a building. Pilot initiates a climb and at the same time starts to build up airspeed by moving forward. One engine fails after some time. In the simulated maneuver, the pilot starts to climb and move forward from hover, and after 6 seconds one engine fails. The simulation results for this maneuver are shown in Fig. 15. The RPM limit is set to 25.65 rad/sec, which is 95% of the normal operating RPM (27 rad/sec). Without the limiting, the results show large RPM droop, but with the limiting the algorithm is successful in forcing the RPM to its desired value.

When both engines fail to operate, the only option for the pilot is to enter autorotation. The pilot should quickly lower the collective in order to avoid a large RPM droop. Further, the pilot needs to adjust the collective in order to avoid over-speeding of the rotor. Figure 16 shows the autorotation results obtained using simulation with and without the limit avoidance system engaged. The results show that if no corrections are made to the collective stick, the pilot runs into the danger of over-speeding the rotor. But, the limiting system guides the pilot to maintain the optimal RPM for recovery from autorotation.

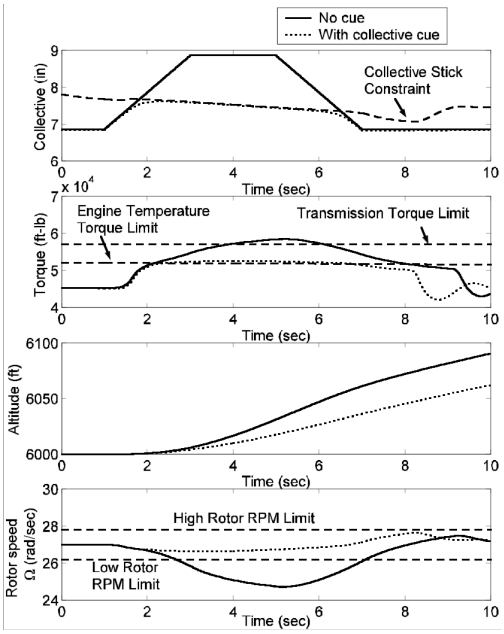

Fig. 13 Engine Temperature limit evaluation with and without limiting.

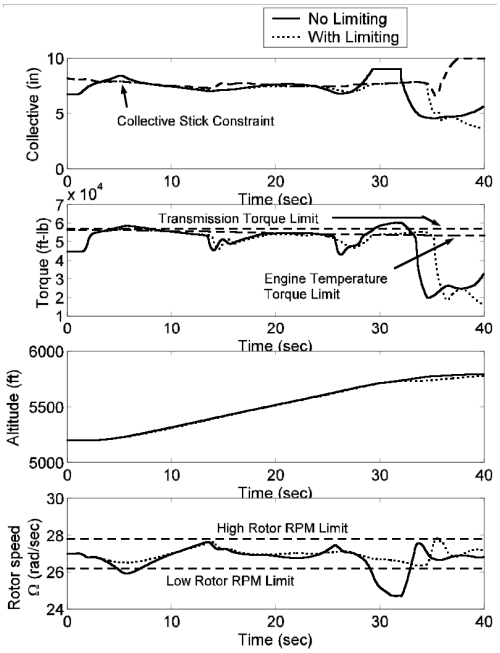

Fig. 14 Continuous torque limit switching from transmission limit to engine temperature limit.

Transient limits are most likely to exceed when the pilot moves the collective stick rapidly. A simple quick bob-up/bob-down maneuver is performed where the pilot starts from hover and moves the stick rapidly through 2 inches. The pilot holds the stick at that position for 5 seconds, then moves the stick rapidly down by 4 inches, holds there for 2 seconds and then returns the stick back to the hover position. Results for this simulation are shown in Fig. 17. Torque and RPM are presented in percentage values. The torque exceeds the limit when no limiting is applied. But, with the limiting, steady-state torque does not exceed the continuous torque limit and also the transient peak is within the desired limits. Also, the RPM shows a large fluctuation when no limiting is applied. These fluctuations can be avoided by a small variation in collective stick when the limiting is applied.

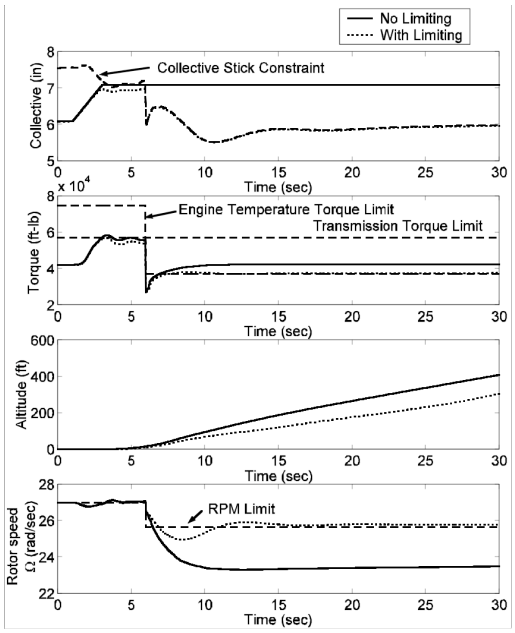

Fig. 15 One Engine Inoperative limit (OEI) with RPM recovery.

The previous results are mainly focused on evaluating the performance of either the steady-state limit avoidance algorithm or the transient limit avoidance algorithm individually. In flight, constraints on the stick can be highly dynamic during aggressive maneuvers. Different limits become critical for different flight conditions and stick motion. The most critical of these limits becomes the constraint on collective stick. Figure 18 demonstrates the dynamic nature of the limits and the effectiveness of the algorithm in determining the critical limit. The figure shows that during 0-10 second period, the stick first hits the RPM limit followed by the transient torque limit and then the continuous torque limit. The same trend is followed for the stick motion between 15-25 second period. During the downward stick motion at 10 seconds, the stick hits the lower RPM limit. The resulting torque and RPM are also shown in the figure. Transient torque, continuous torque and RPM do not exceed the limits. This illustrates the effectiveness of the algorithm in avoiding multiple limits.

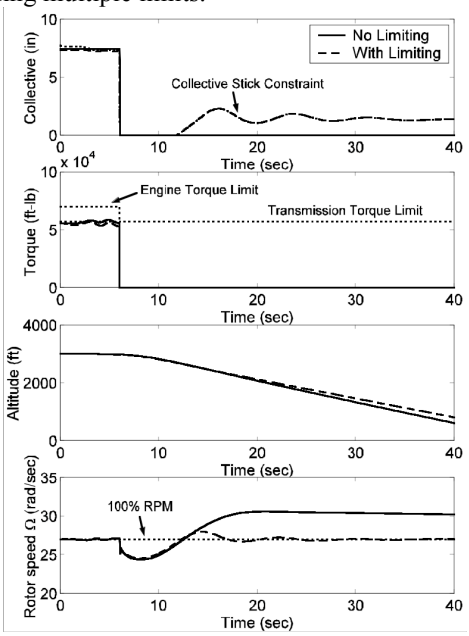

Fig. 16 Autorotation performance with and without limiting.

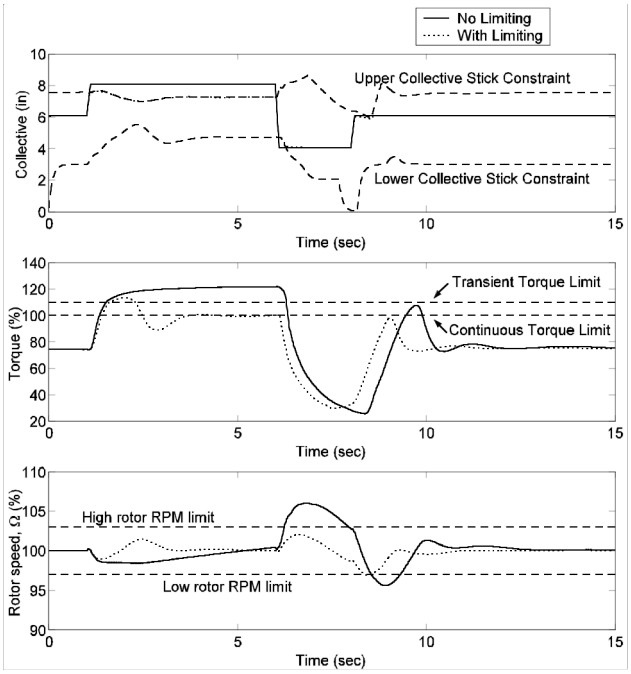

Fig. 17 Evaluation for transient torque and transient RPM limit with and without limiting.

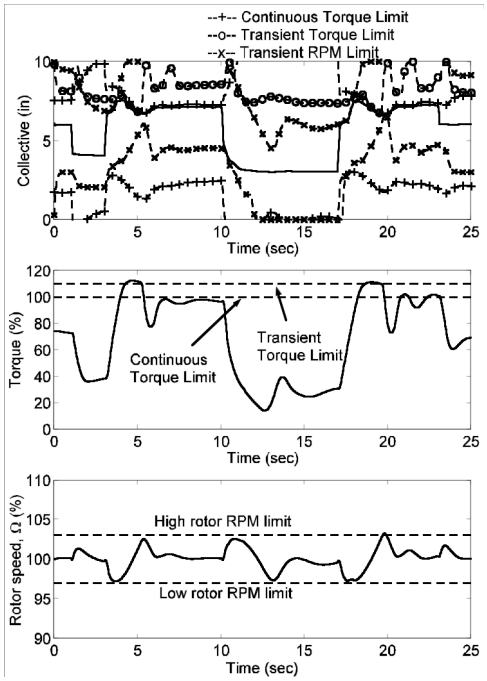

Fig. 18 Interaction of multiple limit boundaries.

X. Conclusion

The objective of the present research was to develop a comprehensive collective axis limit avoidance system suitable for practical implementation in existing rotorcrafts. The system was simultaneously able to handle both continuous and transient limits. A dynamic trim estimation algorithm was used to predict the onset of continuous torque limits, which includes transmission torque limit and engine temperature torque limit. The continuous torque

prediction function (required by this algorithm) was approximated using a neural network. A second order polynomial curve-fit was also evaluated to replace the neural net. Different configurations of input variables were considered for their possible implementation in existing and future rotorcraft. A second-degree polynomial curve-fit was used for approximating engine temperature torque limit. The minimum of the transmission torque limit and the engine temperature torque limit was used for limiting collective stick. A peak response prediction algorithm using linear model of aircraft dynamics was used for predicting stick constraints associated with transient torque and transient RPM limits. Special limits associated with One Engine Inoperative (OEI) recovery and autorotation were evaluated. A new limit over-ride approach for stick limiting was introduced.

The conclusions drawn from this study are

1) When approximating the continuous torque prediction function, using air velocities at the hub and collective and pedal position provides good accuracy but would require expensive sensor upgrading in existing helicopters. With some reduction in accuracy, measurements of total velocity, yaw rate, descent velocity, and collective and pedal position provide a reasonable prediction using existing sensors. Even if low velocity measurements are not available the system has reasonable accuracy.

2) Use of second order curve fits for the torque prediction resulted in substantial reduction in the accuracy of the torque prediction. However, simulation results showed that this method of torque prediction might still be feasible when combined with an adaptive scheme to account for bias errors in the prediction. The simplicity of this algorithm might be desirable for commercial applications which are governed by highly restrictive certification norms for flight control system design.

3) A simple adaptive scheme to account for bias error in the continuous torque prediction using measured torque values seems to provide reasonable results when there are errors in the torque prediction function.

4) The continuous torque prediction algorithm was also effective for avoiding engine temperature limits. Using a simple approximation of the engine temperature limit as a function of ambient temperature and pressure, this torque limit can be substituted for the transmission limit when appropriate. Moreover, the switching of stick constraint from transmission torque limit to engine temperature torque limit at high altitude was found to be smooth in the simulations.

5) The peak response estimation algorithm appeared to be effective in preventing violation of transient torque and rotor speed limits. The algorithm was designed using a linear model in the hover condition, but was shown to be effective over a range of low airspeeds.

6) The simulation results for OEI and autorotation showed that the algorithm may be effective in helping pilots perform emergency procedures in a safe manner. The desired RPM can be maintained by following the stick limit generated by these algorithms.

7) Simulation results showed that the algorithms can be applied for multiple interacting limits in the collective axis and provide cueing or control limiting in a reasonable manner.

8) The limit over-ride approach for stick limiting can be implemented by limiting the stick motion through the AFCS while cueing the pilot using stick shaker cues to distinguish each region in the stick travel. The method could combine the precision of AFCS limiting with limit over-ride capability of stick cueing. Stick shakers are a relatively cheaper upgrade option for conventional collective sticks. The acceptance of such a system would be dependent on handling qualities and pilot preference issues, and thus further piloted simulation analysis of the system is warranted.

Acknowledgments

This research is being funded by the National Rotorcraft Technology Center, under the Penn State Rotorcraft Center of Excellence grant.

References

[1]Howitt, J., "Carefree Maneuvering in Helicopter Flight Control," *Proceedings of the American Helicopter Society 51st Annual Forum*, Vol. 1, American Helicopter Society, Alexandria, VA, May 1995, pp. 287-298.

[2]Whalley, M. S., and Achache, M., "Joint U.S./France Investigation of Helicopter Flight Envelope Limit Cueing," *Proceedings of the American Helicopter Society 52nd Annual Forum*, Vol. 2, American Helicopter Society, Alexandria, VA, June 1996, pp. 1589-1617.

[3]Whalley, M. S., Hindson, W. S., and Thiers, G. G., "A Comparison of Active Sidestick and Conventional Inceptors for Helicopter Flight Envelope Tactile Cueing," *Proceedings of the American Helicopter Society 56th Annual Forum*, Vol. 1, American Helicopter Society, Alexandria, VA, May 2000, pp. 181-204.

[4]Handcock, A., Lane, R., Johns, S., Howitt, J., and Charlton, M., "Benefits of Advanced Control Technology," *Proceedings of the American Helicopter Society 56th Annual Forum, Vol. 1, American Helicopter Society*, Alexandria, VA, May 2000, pp. 147-156.

[5]Mulgund, S. S., and Zacharias, G. L., "A Hybrid Neural Network-Fuzzy Logic Limit Protection System for Rotorcraft," *Proceedings of the AIAA Guidance, Navigation and Control Conference*, AIAA Paper 96-3800, AIAA, July 1996.

[6]Horn, J. F., Calise, A. C., and Prasad, J. V. R, "Flight Envelope Limiting Systems Using Neural Networks," *Proceedings of the AIAA Atmospheric Flight Mechanics Conference*, AIAA, Aug. 1998, pp. 741-751.

[7]Horn, J. F., Calise, A. C., and Prasad, J. V. R, "Development of Envelope Protection Systems for Rotorcraft," *Proceedings of the American Helicopter Society 55th Annual Forum*, Vol. 2, American Helicopter Society, Alexandria, VA, May 1999, pp. 2025-2036.

[8]Horn, J. F., Calise, A. C., and Prasad, J. V. R, "Flight Envelope Limit Detection and Avoidance for Rotorcraft," *Proceedings of the 25th European Rotorcraft Forum*, Vol. 2, National Aerospace Laboratory, Amsterdam, Netherlands, Sept. 1999.

[9]Horn, J. F., Calise, A. C., and Prasad, J. V. R, "Flight Envelope Cueing on a Tilt-Rotor Aircraft Using Neural Network Limit Prediction," *Journal of the American Helicopter Society*, Vol. 46, No. 1, Jan. 2001, pp. 23-31.

[10]Horn, J. F., Calise, A. J., Prasad, J. V. R., "Flight Envelope Limit Detection and Avoidance for Rotorcraft," *Journal of the American Helicopter Society*, Vol. 47, No. 4, Oct. 2002, pp. 253-262.

[11]Horn, J. F., and Sahani, N., "Detection And Avoidance of Main Rotor Hub Moment Limits on Rotorcraft," *Proceedings of the AIAA Atmospheric Flight Mechanics Conference*, AIAA, Aug. 2001, pp. 289-298.

[12]Horn, J. F., and Sahani, N., "Detection And Avoidance of Main Rotor Hub Moment Limits on Rotorcraft," *Journal of Aircraft*, Vol. 41, No. 2, March 2004, pp. 372-379.

[13]Horn, J. F., Sahani, N., Sahasrabudhe, V., Spaulding, R., and Faynberg, A., "Simulation Investigation of a Comprehensive Collective-Axis Tactile Cueing System," *Proceedings of the American Helicopter Society 58th Annual Forum*, Vol. 1, American Helicopter Society, Alexandria, VA, June 2002, pp. 559-568.

[14]Bateman, A., Ward, D., Barron, R., and Whalley, M., "A Piloted Simulation Evaluation of a Neural Network Limit Avoidance System for Rotorcraft," *Proceedings of the AIAA Atmospheric Flight Mechanics Conference*, AIAA, Aug. 1999, pp. 661-673.

[15]Howlett, J., "UH-60A BLACK HAWK Engineering Simulation Program: Volume I – Mathematical Model," NASA CR-177542, USAAVSCOM TR 89-A-001, Sept. 1989.

[16]Fletcher, J., "A Model Structure for Identification of Linear Models of the UH-60 Helicopter in Hover and Forward Flight," NASA TM 110362, USAATCOM TR 95-A-008, Aug. 1995.

[17]Tischler, M. B., and Cauffman, M.G., "Frequency-Response Methods for Rotorcraft System Identification: Flight Applications to BO-105 Coupled Rotor/Fuselage Dynamics," *Journal of the American Helicopter Society*, Vol. 37, No. 3, July 1992.